AIAA-90-2354

UNSTEADY ANALYSIS OF HOT STREAK MIGRATION IN A TURBINE STAGE

Daniel J. Dorney, Roger L. Davis and David E. Edwards
United Technologies Research Center
East Hartford, CT

Nateri K. Madavan
NASA Ames Research Center
Moffett, CA

"Original contains color plates: All DTIC reproductions will be in black and white"

AIAA/SAE/ASME/ASEE
26th Joint Propulsion Conference
July 16-18, 1990 / Orlando, FL

Unsteady Analysis of Hot Streak Migration in a Turbine Stage

Daniel J. Dorney*
Roger L. Davis†
David E. Edwards‡
United Technologies Research Center
East Hartford, CT
and
Nateri K. Madavan §
NASA Ames Research Center
Moffett Field, CA

Abstract

Experimental data taken from gas turbine engines has shown that hot streaks exiting combustors can have a significant impact upon the secondary flow and wall temperature of the first stage turbine rotor. Understanding the secondary flow and heat transfer effects due to combustor hot streaks is essential to turbine designers attempting to optimize turbine cooling systems. A numerical investigation is presented which addresses the issues of multi-blade count ratio and three-dimensionality effects on the prediction of combustor hot streak migration in a turbine stage. The two- and three-dimensional Navier-Stokes analyses developed by Rai *et al* are used to predict unsteady viscous rotor-stator interacting flow in the presence of a combustor hot streak. Predicted results are presented for a two-dimensional 3-stator/4-rotor, a two-dimensional 1-stator/1-rotor, and a three-dimensional 1-stator/1-rotor simulation of hot streak migration through a turbine stage. Comparison of these results with experimental data demonstrates the capability of the three-dimensional procedure to capture most of the flow physics associated with hot streak migration including the effects of combustor hot streaks on turbine rotor surface temperatures.

*Assistant Research Engineer, Theoretical & Computational Fluid Dynamics Group, Member AIAA

†Senior Research Engineer, Theoretical & Computational Fluid Dynamics Group, Member AIAA

‡Senior Research Engineer, Physical & Mathematical Modeling Group, Member AIAA

§Principal Analyst, Sterling Federal Systems, Member AIAA

Nomenclature

a	- Speed of sound
e	- Specific energy
e_t	- Total energy
M	- Mach number
P	- Static pressure
Pr	- Prandtl number
P_T	- Stagnation pressure
Re	- Free stream inlet reference Reynolds number
T	- Static temperature
u	- x component of velocity
U	- Rotor velocity
v	- y component of velocity
w	- z component of velocity
κ	- thermal conductivity
λ	- Second coefficient of viscosity
μ	- First coefficient of viscosity
ρ	- Density
τ	- Shear stress
Ω	- Rotor rotational speed

Subscripts

HS	- Hot streak
i	- Inviscid
L	- Laminar quantity
t	- Stagnation quantity
T	- Turbulent quantity
v	- Viscous
x, y, z	- First derivative with respect to x, y or z
xx, yy, zz	- Second derivative with respect to x, y or z
1	- Inlet quantity
2	- Exit quantity

Introduction

The drive toward low fuel consumption and maximum gas turbine efficiency for commercial aircraft has led to increases in combustor exit temperature which in turn has had a direct impact on the durability of first stage turbine airfoils. In order to keep turbine airfoil wall temperatures below critical levels, complex internal cooling schemes are designed to lay a film of relatively cool air adjacent to the blade. This film cooling air acts as a sealant to keep the high temperature combustor flow from coming in direct contact with turbine airfoil surfaces. During the design of the first stage turbine, flow field analyses which assume a uniform turbine inlet temperature profile are used to predict airfoil surface temperature distributions. These wall temperature distributions are subsequently used to guide the design of internal cooling schemes in terms of defining cooling mass flow requirements and its distribution.

Experimental data taken from actual gas turbine combustors, however, indicate that the flow exiting the combustor has both circumferential and radial temperature gradients. These temperature gradients arise from the combination of the combustor core flow with the combustor bypass and combustor surface cooling flows. It has been shown both experimentally and numerically [1,2] that temperature gradients, in the absence of total pressure non-uniformities, do not alter the flow within the first stage turbine stator but do have significant impact on the secondary flow and wall temperature of the first stage rotor. Combustor hot streaks, which can typically have temperatures twice the free stream stagnation temperature, increase the extent of the secondary flow in the first stage rotor and significantly alter the rotor surface temperature distribution. A combustor hot streak such as this has a greater streamwise velocity than the surrounding fluid and therefore a larger positive incidence angle to the rotor as compared to the free stream. Due to this rotor incidence variation through the hot streak and the slow convection speed on the pressure side of the rotor, the hot streak accumulates on the rotor pressure surface creating a "hot spot".

Both the secondary flow and wall temperature shifting effects due to combustor hot streaks are important phenomena which should be accounted for by turbine designers to increase turbine aerodynamic performance and optimize turbine cooling flow schemes. Without properly accounting for non-uniformities in turbine inlet temperature profiles such as those related to combustor hot streaks, first stage turbine performance and durability could suffer. Computational fluid dynamic simulations of hot streak migration in turbine stage flows can be useful for both increasing the understanding of this phenomena as well as to guide engineers for future experimental investigations. The focus of the current effort has been to perform both two- and three-dimensional rotor/stator interaction numerical simulations which include the effects of combustor hot streaks in order to provide additional insight into the hot streak migration phenomena.

In the present investigation, the two- and three-dimensional unsteady Navier-Stokes analyses of Rai *et al* [3,4] are used to predict the effects of a combustor hot streak on the flow in the first stage of a turbine. Two-dimensional simulations, including 3-stator/4-rotor and 1-stator/1-rotor configurations, have been performed to study the effects of stator/rotor blade count on the time-averaged rotor surface mid-span temperature distribution. In addition, to determine the three-dimensional effects of the hot streak migration on the secondary flow and rotor surface temperature distribution, a three-dimensional 1-stator/1-rotor/1-hot streak simulation has been performed. The results from these computations have been compared to the experimental data reported by Butler *et al* [1] and the computations performed by Rai and Dring [2], Krouthen and Giles [5], and Takahashi and Ni [6,7]. These numerical results and their comparison with the available experimental data sheds new insight into the phenomena of hot streak migration and its effect on first stage turbine aerodynamics and heat transfer.

Numerical Integration Procedure

The governing equations considered in this study are the time dependent, three-dimensional Navier-Stokes equations:

$$U_t + (F_i + F_v)_x + (G_i + G_v)_y + (H_i + H_v)_z = 0 \quad (1)$$

where

$$U = \begin{bmatrix} \rho \\ \rho u \\ \rho v \\ \rho w \\ e_t \end{bmatrix} \quad (2)$$

$$F_i = \begin{bmatrix} \rho u \\ \rho u^2 + P \\ \rho uv \\ \rho uw \\ (e_t + P)u \end{bmatrix} \quad F_v = - \begin{bmatrix} 0 \\ \tau_{xx} \\ \tau_{xy} \\ \tau_{xz} \\ \tau_{hx} \end{bmatrix} \tag{3}$$

$$G_i = \begin{bmatrix} \rho v \\ \rho uv \\ \rho v^2 + P \\ \rho vw \\ (e_t + P)v \end{bmatrix} \quad G_v = - \begin{bmatrix} 0 \\ \tau_{yx} \\ \tau_{yy} \\ \tau_{yz} \\ \tau_{hy} \end{bmatrix} \tag{4}$$

$$H_i = \begin{bmatrix} \rho w \\ \rho uw \\ \rho vw \\ \rho w^2 + P \\ (e_t + P)w \end{bmatrix} \quad H_v = - \begin{bmatrix} 0 \\ \tau_{zx} \\ \tau_{zy} \\ \tau_{zz} \\ \tau_{hz} \end{bmatrix} \tag{5}$$

where

$$\begin{aligned}
\tau_{xx} &= 2\mu u_x + \lambda (u_x + v_y + w_z) \\
\tau_{xy} &= \mu (u_y + v_x) \\
\tau_{xz} &= \mu (u_z + w_x) \\
\tau_{yx} &= \tau_{xy} \\
\tau_{yy} &= 2\mu v_y + \lambda (u_x + v_y + w_z) \\
\tau_{yz} &= \mu (v_z + w_y) \\
\tau_{zx} &= \tau_{xz} \\
\tau_{zy} &= \tau_{yz} \\
\tau_{zz} &= 2\mu w_z + \lambda (u_x + v_y + w_z) \\
\tau_{hx} &= u\tau_{xx} + v\tau_{xy} + w\tau_{xz} + \gamma\mu {P_r}^{-1} e_x \\
\tau_{hy} &= u\tau_{yx} + v\tau_{yy} + w\tau_{yz} + \gamma\mu {P_r}^{-1} e_y \\
\tau_{hz} &= u\tau_{zx} + v\tau_{zy} + w\tau_{zz} + \gamma\mu {P_r}^{-1} e_z \\
e &= \frac{P}{(\rho(\gamma - 1))} \\
e_t &= \rho e + \frac{\rho (u^2 + v^2 + w^2)}{2}
\end{aligned} \tag{6}$$

For the present application, the second coefficient of viscosity is calculated using Stokes' hypothesis, $\lambda = -2/3\mu$. The equations of motion are completed by the perfect gas law.

The viscous fluxes are simplified by incorporating the thin layer assumption [8]. In the current study, viscous terms are retained in the direction normal to the hub surface (z direction) and in the direction normal to the blade surface (y direction). To extend the equations of motion to turbulent flows, an eddy viscosity formulation is used. Thus, the effective viscosity and effective thermal conductivity can be defined as:

$$\begin{aligned}
\mu &= \mu_L + \mu_T \\
\frac{\kappa}{C_p} &= \frac{\mu_L}{P_{rL}} + \frac{\mu_T}{P_{rT}}
\end{aligned} \tag{7}$$

The turbulent viscosity, μ_T, is calculated using the Baldwin-Lomax [8] algebraic turbulence model as applied by Hung and Buning [9] for three-dimensional flows.

The numerical procedure for the three-dimensional analysis consists of a time marching, implicit, third-order spatially accurate, upwind, finite difference scheme. The inviscid fluxes are discretized using a combination of central, forward, and backward differences depending on the local eigenvalues of the flux Jacobians according to the scheme developed by Roe [10]. The viscous fluxes are calculated using standard central differences. The alternate direction, approximate-factorization technique of Beam and Warming [11] is used to compute the time rate changes in the primary variables. An inner Newton iteration can be used to increase stability and reduce linearization errors. For all cases investigated in this study, three Newton iterations were performed at each time step. The numerical procedure used for the two-dimensional analysis is similar to that used in the three-dimensional analysis, except that the inviscid fluxes are discretized according to the scheme developed by Osher [12]. Further details of the two- and three-dimensional numerical techniques can be found in Refs. [2,3,4].

Grid Generation and Geometry

The three-dimensional Navier-Stokes analysis developed by Rai *et al* [2,3,4] uses five zonal grids to discretize the rotor-stator flow field and facilitate relative motion of the rotor. A combination of O- and H-grid sections are generated at constant radial spanwise locations in the blade-to-blade direction extending upstream of the stator leading edge to downstream of the rotor trailing edge. Algebraically generated H-grids are used in the regions upstream of the leading edge, downstream of the trailing edge and in the inter-blade region. The O-grids, which are body-fitted to the surfaces of the airfoils and generated using an elliptic equation solution

procedure, are used to properly resolve the viscous flow in the blade passages and to easily apply the algebraic turbulence model. Computational grid lines within the O-grids are stretched in the blade-normal direction with a fine grid spacing at the wall. The combined H- and O- overlaid grid sections are stretched in the spanwise direction away from the hub and tip regions with a fine grid spacing located adjacent to the hub and tip. An O-grid structure is used in the region between the rotor blade and the tip endwall in the tip clearance region. Grid generation for the two-dimensional analysis is similar to that for the three-dimensional procedure except that the O-grids are patched, rather than overlaid, into the H-grids.

Boundary Conditions

The theory of characteristics is used to determine the boundary conditions at the stator inlet and rotor exit. For subsonic inlet flow, the total pressure, v and w velocity components and the downstream running Riemann invariant, $R_1 = u + \frac{2a}{\gamma-1}$, are specified while the upstream running Riemann invariant, $R_2 = u - \frac{2a}{\gamma-1}$, is extrapolated from the interior of the computational domain. Inlet flow boundary conditions within the hot streak region are updated using Riemann invariants where the velocity and speed of sound reflect the static and stagnation temperature increase in the hot streak. The static and total pressure in the hot streak is assumed to be equal to that of the undisturbed inlet flow. For subsonic outflow the pressure ratio P_2/P_{t1} is specified while the v and w velocity components, entropy, and the downstream running Riemann invariant are extrapolated from the interior of the computational domain. Absolute no-slip boundary conditions are enforced at the hub and tip endwalls of the stator region, along the surface of the stator, and along the outer casing (tip endwall) of the rotor. Relative no-slip boundary conditions are imposed at the hub and along the surface of the rotor. Periodicity is enforced along the outer boundaries of the H-grids in the circumferential (θ) direction. In the present, study the flow is assumed to be adiabatic.

Dirichlet conditions, in which the time rate change in the vector U of Eq. (2) is set to zero, are imposed at the grid interface boundaries located between the stator and rotor H-grids and at the overlaid boundaries of the O- and H-grids in the stator and rotor regions. The flow variables of U at zonal boundaries are explicity updated after each time step by interpolating values from the adjacent grid. Because of the explicit application of the zonal boundary conditions, large time steps necessitate the use of more than one Newton iteration. The zonal boundary conditions are non-conservative, but for subsonic flow this should not affect the accuracy of the final flow solution. Further information describing the implementation of the boundary conditions can be found in Refs. [2,3,4,13].

Results

A numerical investigation of hot streak migration has been conducted in which predicted results using the two- and three-dimensional versions of the current Navier-Stokes procedure (ROTOR2, ROTOR3) have been compared with experimental data reported by Butler *et al* [1]. The turbine airfoil geometry used in both the two- and three-dimensional analyses consists of the first stage of the UTRC Large Scale Rotating Rig (LSRR) [1,14] which includes 22 stator airfoils and 28 rotor airfoils. An accurate simulation of this configuration requires at least 11 stator and 14 rotor airfoils. For the 1-stator/1-rotor two- and three-dimensional simulations, the rescaling strategy of Madavan *et al* [15] is used to reduce the number of airfoils to one stator and one rotor. The stator was scaled down by a factor of (22/28) and it was assumed that there were 28 stator airfoils. The pitch to chord ratio of the stator was not changed. This is different than the scaling strategy used by Rai and Dring [2] in which the rotor was scaled by a factor of (28/22) and it was assumed there were 22 rotor airfoils. For the two-dimensional 3-stator/4-rotor simulation, a rescaling strategy was used to reduce the number of airfoils to 3 stators and 4 rotors. In this case it was assumed that there were 21 stator airfoils and 28 rotor airfoils and the stators were enlarged by the factor (22/21).

In the experimental study [1], one hot streak was introduced through a circular pipe at 40% span, and midway between, two stator airfoils of the LSRR. The temperature of the hot streak was twice that of the surrounding inlet flow, whereas the hot streak static and stagnation pressures were identical to the free stream. The hot streak was seeded with CO_2 and the path of the hot streak determined by measuring CO_2 concentrations at various locations within the turbine stage. In the two-dimensional 1-stator/1-rotor simulation and three-dimensional 1-stator/1-rotor simulation, one hot streak is introduced to the inlet of each stator passage. For the two-dimensional 3-stator/4-rotor simulation, one hot streak is introduced to the inlet of every third stator passage. The temperature of the hot streak in the current investigation is 1.2 times the temperature of the surrounding inlet flow. For the two-dimensional

3-stator/4-rotor simulation, the hot streak was introduced over a distance equal to one quarter of a stator pitch and centered at the mid-gap position between the second and third stator. For the two-dimensional 1-stator/1-rotor simulation, the hot streak was introduced over one quarter of the stator pitch and centered at mid-gap. In the three-dimensional simulation, the hot streak was introduced through a two inch diameter circular region which corresponds to the two inch diameter pipe used in the experiment [1]. The center of the hot streak was located at the mid-gap, 40% span location. In both the two- and three-dimensional calculations, the temperature profile used at the stator inlet to simulate the combustor hot streak consisted of a hyperbolic tangent (step-like) distribution.

A 15% axial gap between the stator and rotor was used in both the two-dimensional and three-dimensional simulations, while the experimental configuration had a 65% axial gap. It has been demonstrated [16] that the axial gap has no significant impact on either the time-averaged pressure distributions or time-averaged heat transfer coefficients on the stator or rotor. Secondary flow and other viscous mechanisms, however, can be affected by the stator/rotor axial gap. The inlet Mach number to the stator was 0.07 and the inlet flow was assumed to be axial. The rotor rotational speed was 410 rpm. The experimental flow coefficient was $\phi = u/U = .68$, while the numerical simulations held a flow coefficient of $\phi = .78$. The free stream Reynolds number was 100,000 per inch. A pressure ratio of $P_2/P_{t1} = .963$ was determined from the inlet total pressure and the static pressure measured in the rotor trailing-edge plane.

Two-Dimensional Simulations

A two-dimensional 3-stator/4-rotor and a 1-stator/1-rotor hot streak simulation have been performed as part of a numerical investigation into the effects of stator to rotor blade count on hot streak migration and time-averaged wall temperature distributions. The two-dimensional calculations performed during this investigation were computed on a four processor Alliant FX-80 mini-supercomputer. Typical calculations required .00191 seconds per grid point per iteration computation time. For both two-dimensional simulations, approximately six cycles at 3000 iterations per global cycle were needed to obtain a time-periodic solution. A global cycle corresponds to the rotor blade rotating through an angle of $2\pi/N$ where N is the number of stator blades (i.e. N=3 and N=1).

For the two-dimensional 3-stator/4-rotor simulation, each of the three stator grids was constructed with 101 × 31 (streamwise × tangential) grid points in the O-grid and 71 × 51 grid points in the H-grid. Each of the four rotor grids was constructed with 101 × 31 grid points in the O-grid and 75 × 51 grid points in the H-grid. A total of 48,080 grid points and an average blade wall spacing of 2.0×10^{-4} inches were used in this simulation. For the two-dimensional 1-stator/1-rotor simulation, the stator zone was constructed with 101 × 31 grid points in the O-grid and 75 × 31 grid points in the H-grid. The rotor zone was constructed with 101 × 31 grid points in the O-grid and 71 × 31 grid points in the H-grid. A total of 10,788 grid points and an average wall spacing of 2.0×10^{-4} inches were used in this calculation. Examples of the grid topology used in the two-dimensional simulations are shown in Refs. [2,4].

Results of the two-dimensional simulations have been compared with the time-averaged experimental data [1,14]. Figure 1 shows a comparison of the time-averaged stator surface pressure distribution predicted by the numerical analysis for the 3-stator/4-rotor and 1-stator/1-rotor configurations with experimental data reported by Dring *et al* [14]. The time-averaged pressure coefficient is defined as:

$$C_p = \frac{P_{avg} - P_{t1}}{\frac{1}{2}\rho_1 U^2} \tag{8}$$

where P_{avg} is the local time-averaged pressure, P_{t1} is the inlet total pressure, ρ_1 is the average inlet free stream density, and U is the rotor velocity. The predicted results for the 3-stator/4-rotor and 1-stator/1-rotor configurations both exhibit good agreement with the experimental data. Figure 2 presents a comparison of the predicted results of the two simulations with the experimental time-averaged surface pressure data for the rotor. Excellent agreement exists between the numerical predictions and the data. The predicted results shown in Figs. 1 and 2 are also in good agreement with those reported by Rai *et al* [2,4] for a similar 1-stator/1-rotor configuration with and without a hot streak. These figures substantiate that the effect of the hot streak on the time-averaged pressure fields of the stator and rotor is negligible since the static and stagnation pressure of the hot streak is identical to that of the free stream.

A measure of the unsteadiness of the flow can be obtained by evaluating the size of the surface pressure fluctuations of the stator and rotor. The pressure fluctuations can be quantified through the use of an unsteady pressure amplitude coefficient defined by:

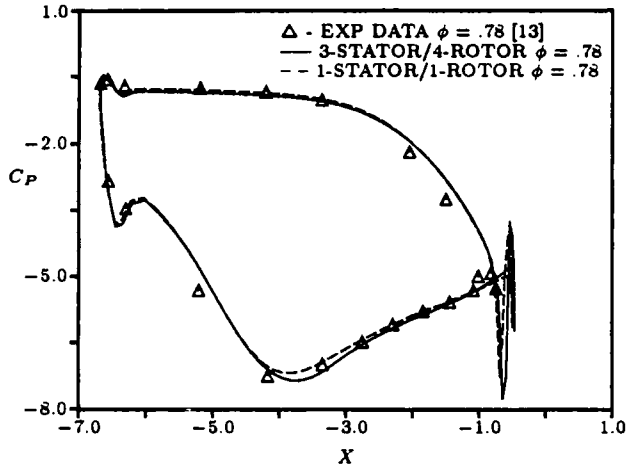

Figure 1: Predicted and experimental blade loading for the stator (2-D)

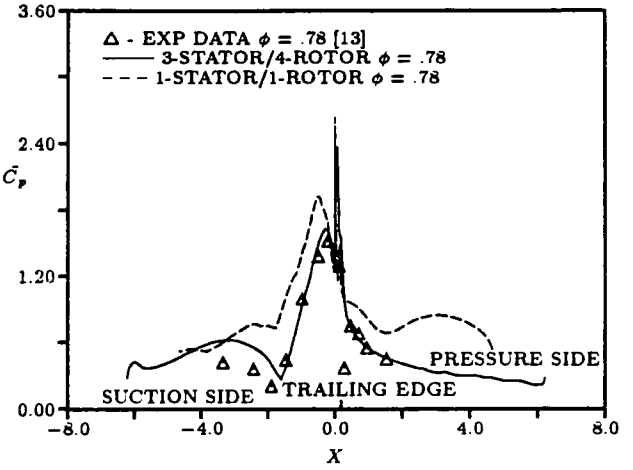

Figure 3: Pressure amplitude coefficient distribution for stator (2-D)

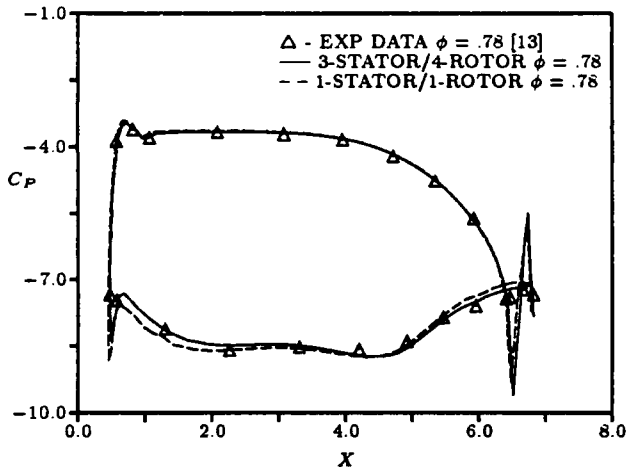

Figure 2: Predicted and experimental blade loading for the rotor (2-D)

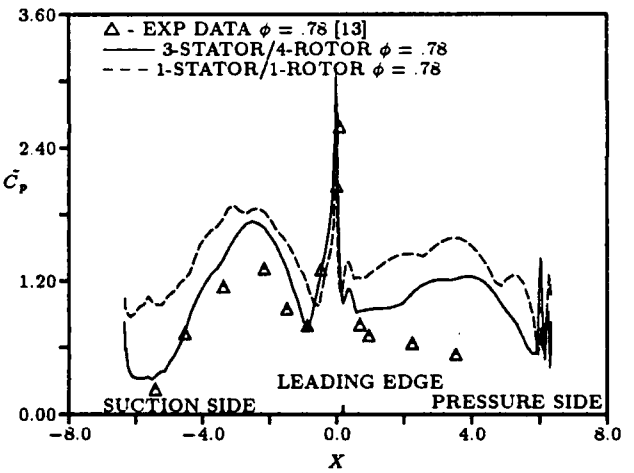

Figure 4: Pressure amplitude coefficient distribution for rotor (2-D)

$$\tilde{C}_p = \frac{P_{max} - P_{min}}{\frac{1}{2}\rho_1 U^2} \qquad (9)$$

Figure 3 illustrates the predicted and experimental values of the unsteady pressure amplitude coefficient for the surface of the stator. Good agreement exists between the predicted 3-stator/4-rotor results and the experimental data. This figure shows that the amplitude of the pressure variations is small on the stator except near the trailing edge. The predicted results for the 1-stator/1-rotor configuration show larger pressure fluctuations than for the 3-stator/4-rotor configuration and the experimental data. The larger fluctuations are due to pressure signals which do not decay for even blade count configurations [4] and the reflective exit boundary conditions used in the numerical procedure. Fig-

ure 4 illustrates the predicted and experimental values of the unsteady pressure amplitude coefficient for the rotor. Good agreement exists between the predicted 3-stator/4-rotor results and the experimental data except near the pressure surface trailing edge, where the pressure variations are greater than those observed experimentally. Again, the predicted pressure fluctuations for the 1-stator/1-rotor configuration are larger than those predicted in the 3-stator/4-rotor configuration as well as the experimental data. Figures 1-4 illustrate that the stator/rotor blade count ratio has little effect on the time-averaged pressure field, but has considerable impact on the unsteady pressure field.

Figure 5 shows the predicted 3-stator/4-rotor and 1-stator/1-rotor time-averaged temperature coefficient distributions compared with the experimental data reported by Butler *et al* [1] for the rotor. Also included in Fig. 5 are the two-dimensional numerical results of Rai and Dring [2] and Krouthen and Giles (rescaled) [5]. The temperature coefficient, $\bar{C}_T$, is defined as [2,7]:

$$\bar{C}_T = \frac{T - T_1}{T_{avg_{rle}} - T_1} \tag{10}$$

where T is the *time-averaged* local temperature and $T_{avg_{rle}}$ is the time-averaged mid-span temperature at the rotor leading edge. This definition of the temperature coefficient facilitates comparison between the present solutions and the predicted results of Rai and Dring [2], Krouthen and Giles [5], and the experimental data [1]. The time-averaged temperature coefficient distribution for the 1-stator/1-rotor hot streak calculation is essentially the same as that reported by Rai and Dring [2] except for a small difference on the pressure surface. The discrepancies on the pressure surface are probably due to the difference in airfoil scaling strategies discussed eariler. The predicted time-averaged temperature coefficient distribution for the pressure surface of the 3-stator/4-rotor simulation is similar to that of the 1-stator/1-rotor calculation, but the suction surface temperature coefficient distribution shows lower time-averaged temperatures than that predicted in the 1-stator/1-rotor calculation. The lower suction surface temperatures predicted in the 3-stator/4-rotor simulation may be the result of introducing one hot streak every third stator passage instead of a hot streak in each stator passage. The temperature coefficient distribution obtained by Krouthen and Giles [5] is similar to the present 3-stator/4-rotor prediction.

The segregation of the hot gases to the pressure side of the rotor passage has been, until this time, believed to be caused soley by the relative inlet angle difference between the hot streak and the surrounding fluid at the inlet to the rotor passage [1]. Results of the two-dimensional simulation confirm experimental observations which indicate that the static pressure, total pressure, and absolute flow angle are the same in the hot streak as in the surrounding fluid at the stator exit. The difference in the total temperature between the hot streak and the surrounding fluid results in an absolute velocity difference equal to the square root of the ratio of the hot streak and surrounding fluid temperatures. In the relative frame, a difference in the rotor relative inlet angle and velocity results. As a result, the hot streak fluid moves towards the pressure surface at a higher relative velocity compared to the surrounding fluid [1]. Time-averaged static temperature contours for the rotor passage of the two-dimensional 3-stator/4-rotor configuration are shown in Fig. 6. Although the hot streak fluid accumulates near the pressure side of the rotor, the hot fluid does *not* penetrate the boundary layer to the surface of the rotor blade. The thin layer of cooler fluid which exists between the hot fluid and rotor pressure surface helps explain the flat temperature coefficient profiles shown in Fig. 5 for the two-dimensional solutions.

All of the two-dimensional numerical simulations shown in Fig. 5 predict nearly equal time-averaged temperatures on the pressure and suction surfaces and fail to predict the increased rotor pressure surface temperatures observed experimentally. Clearly, an additional mechanism other than the rotor incidence variation through the hot streak is accounting for the experimentally observed temperature rise on the pressure side of the airfoil.

To gain better insight into the unsteady phenomena within the turbine stage, animated sequences of the flow field were created. Figure 7 shows the temperature field at one instant in time during the animated sequence. The hot streak is undisturbed as it migrates through the stator passage, except that the width of the hot streak decreases due to flow acceleration. The geometry of the turbine rotor blades is such that the hot streak impinges first on the suction surface, then wraps around the leading edge and moves along the pressure surface. As a result of this movement, the rotor pressure surface temperature does not peak until some time after the rotor blade interacts with the hot streak. The hot streak assumes a V shape as it continues to convect through the rotor passage.

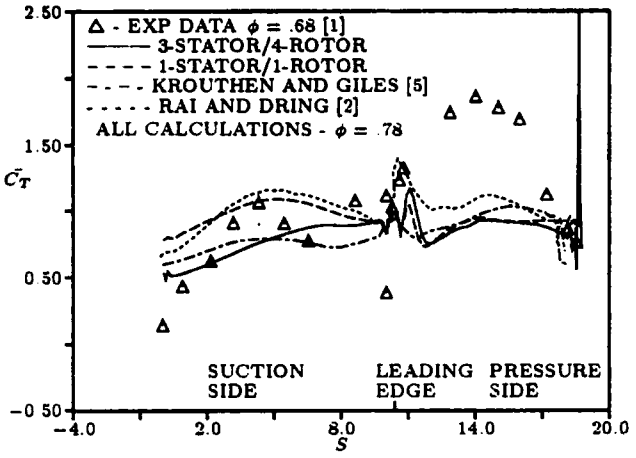

Figure 5: Predicted and experimental time-averaged surface temperature for rotor (2-D)

Figure 6: Time averaged static temperature contours for 2-D hot streak (3-stator/4-rotor)

Three-Dimensional Simulation

A 1-stator/1-rotor three-dimensional hot streak simulation with a hot streak temperature 20 percent greater than the free stream temperature has also been performed to establish the three-dimensional hot streak mi-

Figure 7: Static temperature contours for 2-D hot streak

gration effects on the time-averaged rotor surface temperature distribution. The three-dimensional calculation was performed on the NAS Cray 2 supercomputer located at the NASA Ames Research Center. This calculation required .000263 seconds per grid point per iteration computation time. Seven cycles at 2000 iterations per cycle were needed to obtain a time-periodic solution.

For the three-dimensional simulation, the stator grid system was constructed with 101 x 21 grid points in each spanwise O-grid and 58 x 31 grid points in each spanwise H-grid. The rotor grid system was constructed with 101 x 21 grid points in each spanwise O-grid and 60 x 31 grid points in each spanwise H-grid. A total of 51 O-H grid planes were distributed in the spanwise direction. The rotor region had a tip clearance grid system that contained 101 x 11 grid points in each of 7 spanwise locations. A total of 410,677 grid points were used in the three-dimensional simulation. A wall spacing of 5.0×10^{-4} inches was used in the blade-to-blade direction, while a wall spacing of 3.0×10^{-2} inches was used in the spanwise direction. The experimental rotor has a tip gap equal to 1% of the rotor span, while the tip clearance in the three-dimensional simulation is equal to 3.9% of the rotor span. Illustrations of the three-dimensional computational grid topology can be found in Refs. [3,15].

As part of the numerical investigation, the predicted

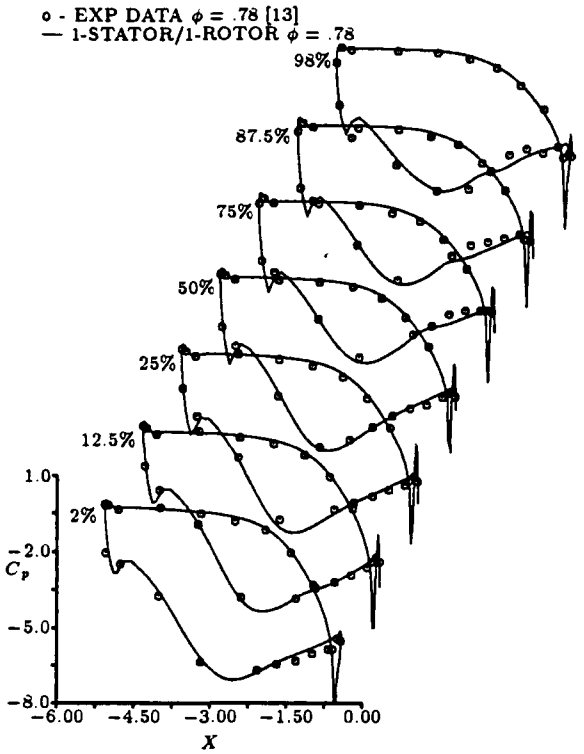

Figure 8: Time-averaged pressure coefficient distribution for stator

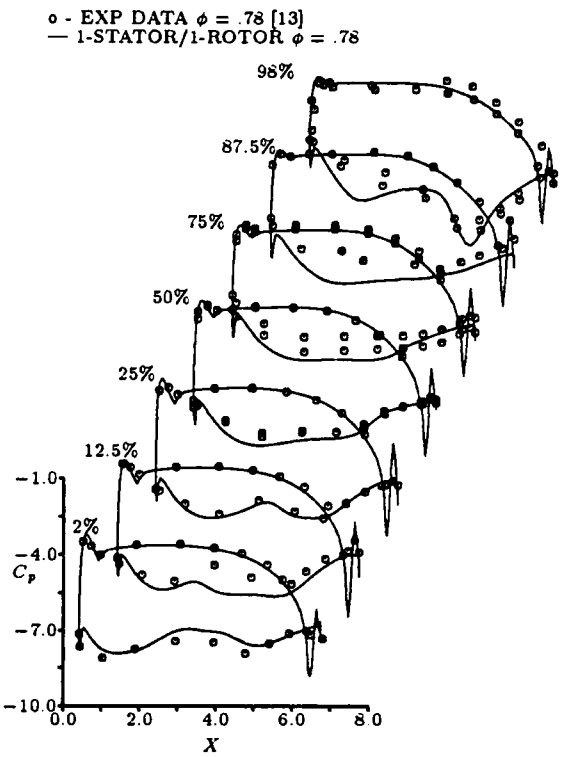

Figure 9: Time-averaged pressure coefficient distribution for rotor

unsteady pressures and temperatures have been time-averaged and compared to the experimental data [14]. Figure 8 illustrates the predicted and experimental time-averaged pressure coefficient distributions on the stator at 2, 12.5, 25, 50, 75, 87.5 and 98% span locations. In general, there is good agreement between the predicted results and the experimental data. The predicted results also agree well with those presented by Rai [3] and Madavan *et al* [15].

Predicted and experimental time-averaged pressure coefficient distributions for the rotor at the 2, 12.5, 25, 50, 75, 87.5 and 98% span locations are shown in Fig. 9. Good agreement between the predicted results and the experimental data is observed from the hub to the mid-span location of the rotor. Some discrepancies between the predicted and the experimental pressure distributions are evident on the suction surface of the rotor, however, from the mid-span location out to the tip. These discrepancies are probably caused by the stronger secondary flows which arose in the calculation due to the relatively large tip clearance.

Figure 10 shows the predicted and experimental values of the unsteady pressure amplitude coefficient for the mid-span section of the stator. The predicted suction surface pressure fluctuations near the trailing edge are smaller than those of the experimental data and the two-dimensional results shown in Fig. 3. In addition, the pressure amplitude coefficient on the pressure surface does not rise near the trailing edge compared to the experimental data and predicted two-dimensional results (Fig. 3). Figure 11 illustrates the predicted and experimental values of the unsteady pressure amplitude coefficient for the mid-span section of the rotor. Fair agreement exists between the predicted results and experimental data as the predicted results show larger pressure fluctuations than those observed experimentally and predicted two-dimensionally (Fig. 4). The stator and rotor pressure amplitude results shown in Figs. 10 and 11 are similar to the coarse grid predictions of Rai [3]. Madavan *et al* [15] showed that the pressure amplitudes on both the stator and rotor are sensitive to the computational grid density. The results shown in Figs. 10 and 11 are predicted using the same fine computational grid density as Madavan*et al* [15]. However, the wall spacing used in the current calculation was increased in order to yield a unif rm grid near

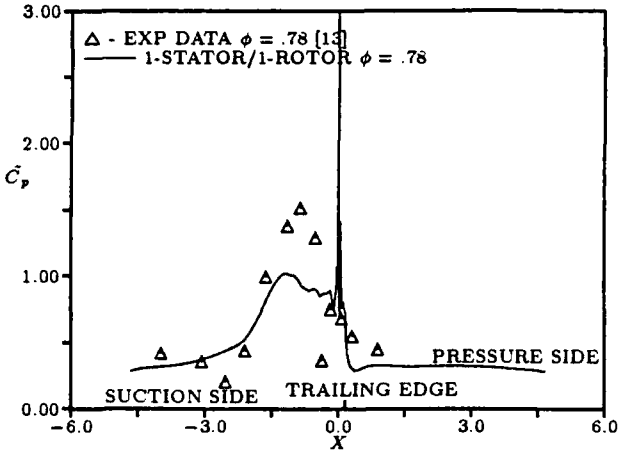

Figure 10: Pressure amplitude coefficient for mid-span stator section

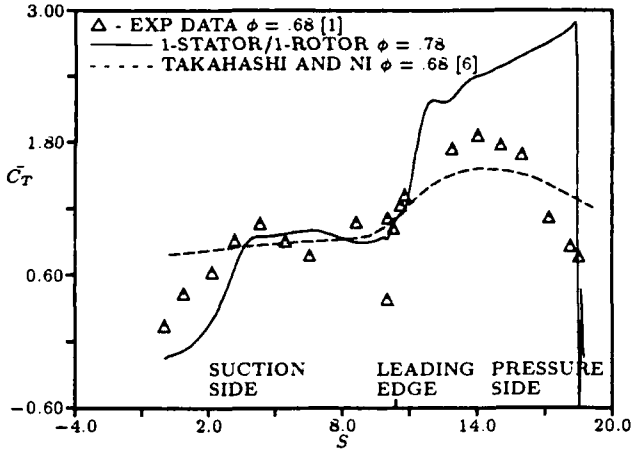

Figure 12: Predicted and experimental time-averaged surface temperature for rotor mid-span section

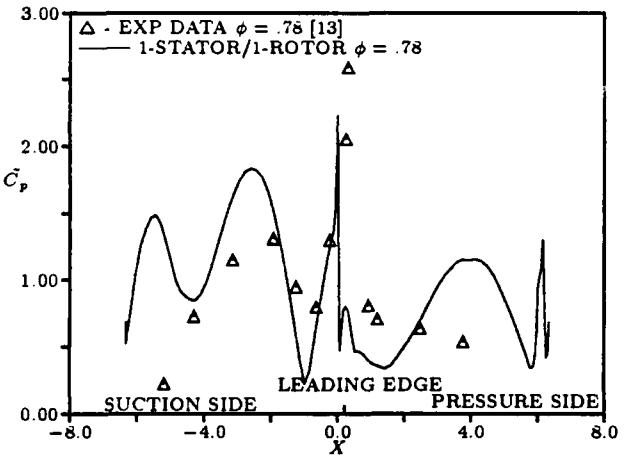

Figure 11: Pressure amplitude coefficient for mid-span rotor section

mid-span/mid-gap, which was necessary to maintain a circular hot streak. Comparison between the current results and those of Rai [3] and Madavan*et al* [15] show that the predicted pressure amplitude is not only sensitive to computational grid density, but also to the spanwise distribution of grid points.

Figure 12 illustrates the predicted and experimental values of the time-averaged temperature coefficient distribution for the mid-span section of the rotor. Also included in Fig. 12 are the three-dimensional inviscid (with viscous modelling) results of Takahashi and Ni [6,7]. The three-dimensional simulation correctly predicts that the pressure surface of the rotor is subject to much higher time-averaged temperatures than the suction surface. In addition, the present three-dimensional calculation correctly predicts the rapid fall-off in the time-averaged temperature on the suction surface. Comparison between the current results and the solution of Takahashi and Ni shows that both three-dimensional techniques predict similar trends with the current Navier-Stokes technique providing more detailed agreement with the experimental data. This comparison, along with the two-dimensional results, implies that the interaction between the secondary and wall layer flows in the rotor passage and the hot streak is an important factor in the time-averaged rotor surface temperature distribution. Furthermore, this comparison highlights the importance of accurately predicting the secondary and wall layer flows through the turbine stage in order to correctly predict the rotor surface temperature distributions.

The predicted rotor surface temperature coefficient contours are illustrated in Fig. 13, while the experimental contours [1] are shown in Fig. 14. The predicted contour patterns are similar to the experimental contours, except near the pressure surface trailing edge where the numerical contours do not close as the experimental data indicates. This difference between

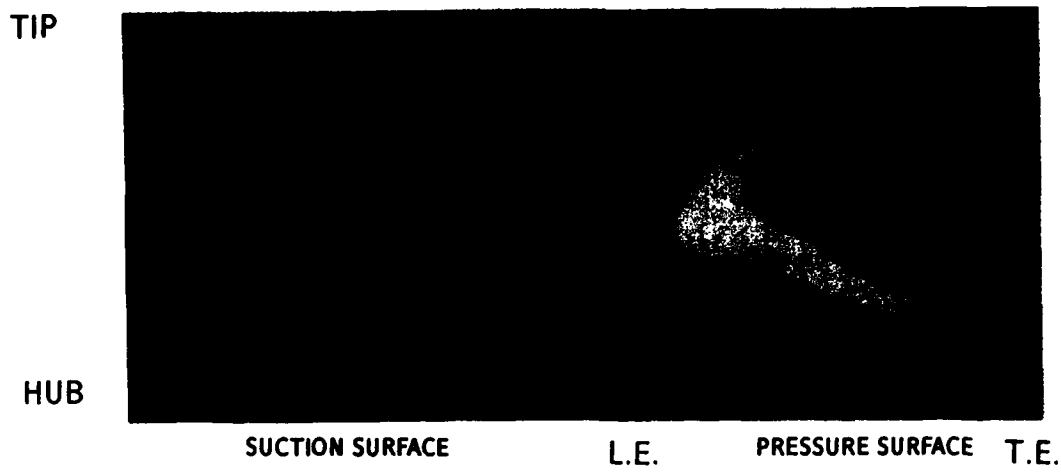

Figure 13: Predicted time-averaged surface temperature contours for rotor airfoil

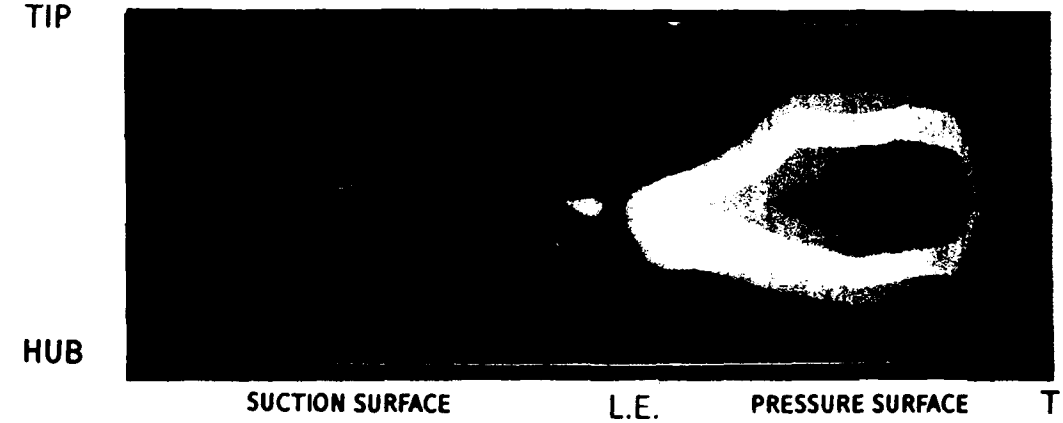

Figure 14: Experimental time-averaged surface temperature contours for rotor airfoil [1]

the prediction and the experiment coincides with that shown in Fig. 12 for the mid-span pressure surface near the trailing edge. This discrepancy is probably due to the difference in flow coefficients between the simulation ($\phi = .78$) and the experiment ($\phi = .68$), resulting in a rotor inlet flow with 5 degrees more positive incidence in the simulation than in the experiment. Both the numerical and experimental results illustrate that the hot fluid spreads over the entire pressure surface of the rotor, while on the suction surface the hot fluid is generally confined to the mid-span region of the rotor surface.

As was performed for the two-dimensional simulation, animated sequences of the flow field were created from results of the three-dimensional simulation. A sequence from the animation of the $T = 1.05$ temperature isotherm at four instants in time during a global cycle are shown in Figs. 15 and 16. These four instants in time correspond to 0, 25, 50 and 75% of the global cycle, where the global cycle is equal to the rotor blade moving a distance equal to one stator pitch. Figure 15 shows the isotherm from a viewing position that displays the pressure surface of the stator blades and the suction surface of the rotor blades. Figure 16 shows the isotherm from a viewing position that displays the suction surface of the stator blades and the pressure surface of the rotor blades. This sequence of pictures illustrates the migration of the hot streak through the stator passage and how it is broken into discrete spherical eddies as it interacts with the passing rotor blades. The hot fluid remains on the pressure surface of the rotor for a long period of time after it encounters the hot streak, eventually migrating towards the pressure surface tip, where it leaks over onto the suction surface.

Conclusions

Experimental studies have shown that combustor hot streaks can significantly affect the secondary flows and wall temperature of the first stage turbine rotor. To gain insight into the secondary flow and heat transfer effects on a first stage rotor due to a combustor hot streak, numerical simulations of hot streak migration through a turbine stage have been performed. The goal of these simulations has been to understand the physical mechanisms which control the migration of hot streaks through a turbine stage and lead to "hot spots" on the rotor pressure surface.

Results have been presented for both two-dimensional and three-dimensional simulations of hot streak migration through a turbine stage. The predicted results from

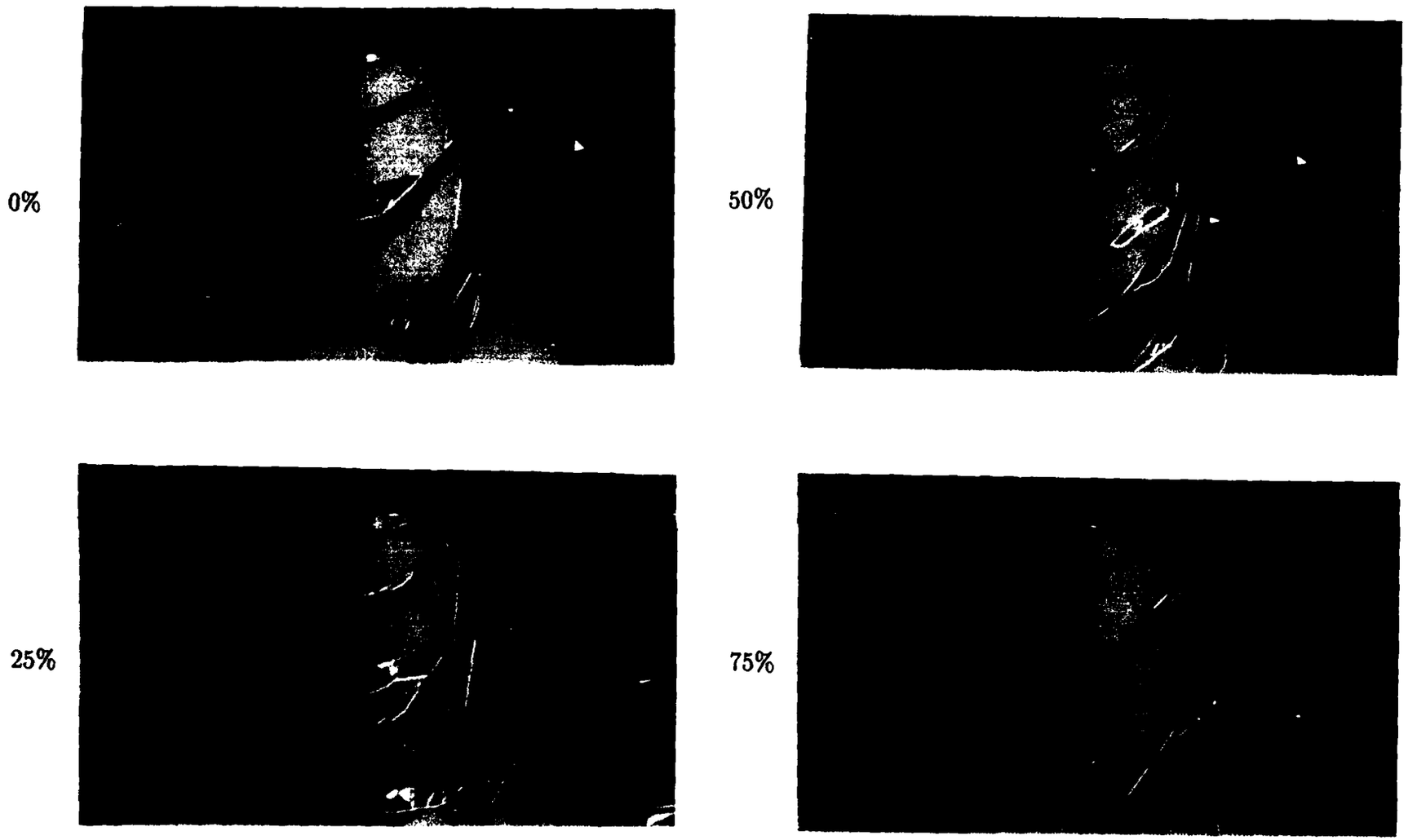

Figure 15: $T = 1.05$ Isotherm for 3-D hot streak (rotor suction side)

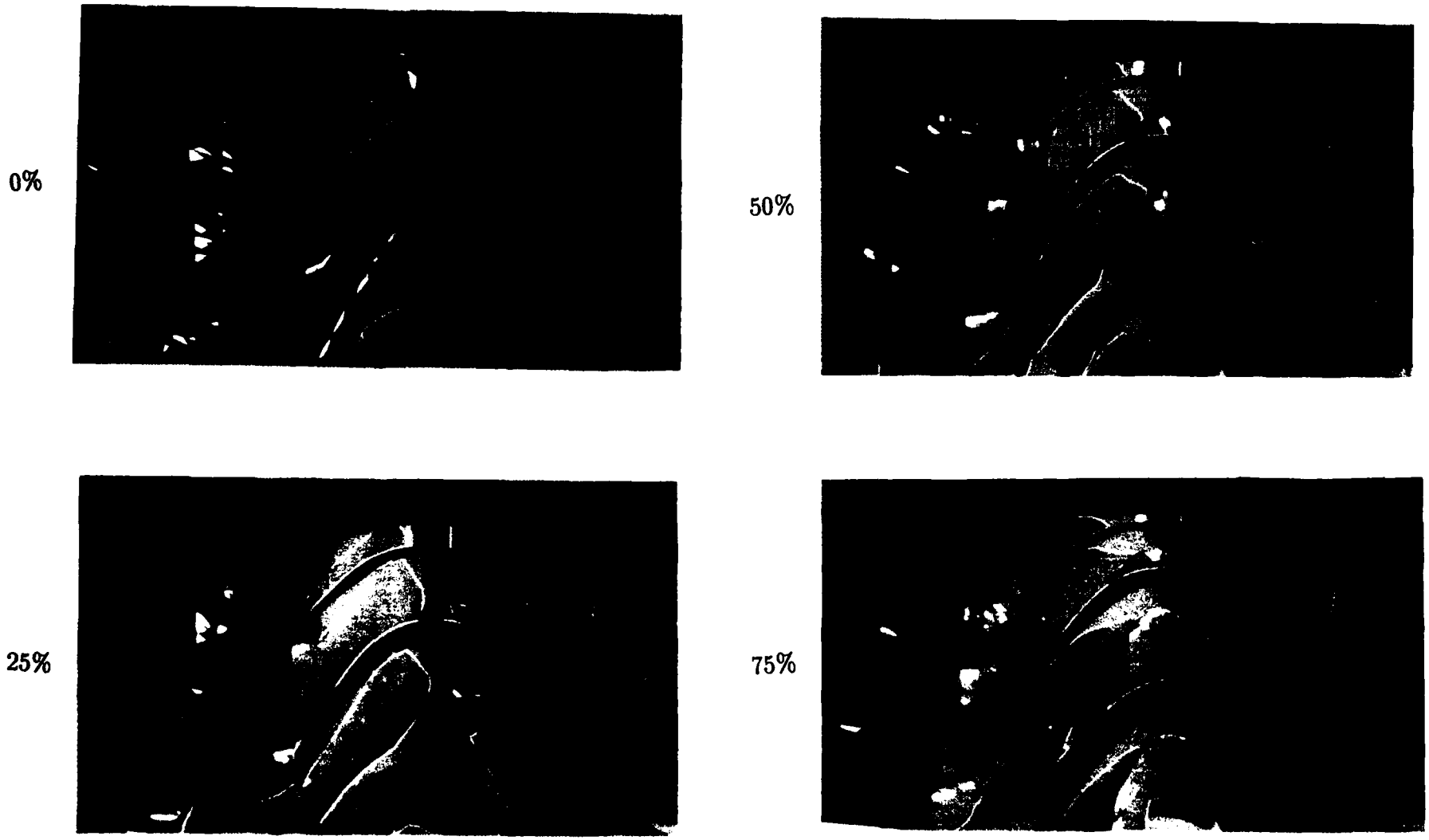

Figure 16: $T = 1.05$ Isotherm for 3-D hot streak (rotor pressure side)

the two-dimensional simulations indicate that blade count ratio has little effect on predicted time-averaged surface pressure and temperature distributions, but a substantial effect on the unsteady flow characteristics. These two-dimensional simulations fail to predict the experimentally observed increase in time-averaged pressure surface temperatures due to the hot streak. Results of the three-dimensional hot streak simulation, however, confirm experimental observations that high temperature hot streak fluid accumulates on the pressure surface of the rotor blades, resulting in a high time-averaged surface temperature "hot spot". The inability of the two-dimensional simulations to predict the increased rotor pressure surface temperatures underscores the importance of including three-dimensional viscous effects. In addition, the influence of secondary flows on the predicted three-dimensional migration pattern of the hot streak has been shown to be consistent with experimental data.

Acknowledgements

This work was supported by the Naval Air Systems Command under NAVAIR contract N00014-88-0677 from the office of George Derderian with Raymond Shreeve of the Naval Post Graduate School acting as technical monitor and the United Technologies Research Center under the Corporate Research Program. The authors would like to thank Man Mohan Rai and Linda Haines of the NASA Ames Research Center for assistance in computational aspects of this investigation. The authors appreciate the helpful discussions with Robert Dring and Dave Joslyn of the United Technologies Research Center and Om Sharma, Ron Takahashi, and Bob Ni of Pratt & Whitney concerning interpretion of the experimental results. The authors would also like to thank Diane Rodimon of the United Technologies Research Center for help with the graphic visualization.

References

[1] Butler, T. L., Sharma, O. P., Joslyn, H. D., and Dring, R. P., "Redistribution of an Inlet Temperature Distortion in an Axial Flow Turbine Stage," *Journal of Propulsion and Power*, Vol. 5, January-February, 1989.

[2] Rai, M. M. and Dring, R. P., "Navier-Stokes Analyses of the Redistribution of Inlet Temperature Distortions in a Turbine," *Journal of Propulsion and Power*, Vol. 6, May-June 1990.

[3] Rai, M. M., "Three-Dimensional Navier-Stokes Simulations of Turbine Rotor-Stator Interaction," *Journal of Propulsion and Power* Vol. 5, May-June, 1989.

[4] Rai, M. M. and Madavan, N. K., "Multi-Airfoil Navier-Stokes Simulations of Turbine Rotor-Stator Interaction," AIAA Paper 88-0361, 1988.

[5] Krouthen, B., and Giles, M., "Numerical Investigation of Hot Streaks in Turbines," AIAA Paper 88-3015, July, 1988.

[6] Takahashi, R. and Ni, R. H., "Unsteady Euler Analysis of the Redistribution of an Inlet Temperature Distortion in a Turbine," AIAA Paper 90-2262, July, 1990.

[7] Sharma, O. P., Pickett, G. F., and Ni, R. H., "Assessment of Unsteady Flows in Turbines," ASME Paper 90-GT-150, 1990.

[8] Baldwin, B. S. and Lomax, H., "Thin-Layer Approximation and Algebraic Model for Separated Turbulent Flows," AIAA Paper 78-257, January, 1978.

[9] Hung, C. M. and Buning, P. G., "Simulation of Blunt-Fin-Induced Shock-Wave and Turbulent-Layer Interaction," *Journal of Fluid Mechanics*, Vol. 154, pp.163-185, 1985.

[10] Roe, P. L., "Approximate Riemann Solvers, Parameter Vectors, and Difference Schemes," *Journal of Computational Physics*, Vol. 43, pp.357-372, 1981.

[11] Beam, R. M. and Warming, R. F., "An Implicit Factored Scheme for the Compressible Navier-Stokes Equations," AIAA Paper 77-645, 1977.

[12] Chakravarthy, S. and Osher, S., "Numerical Experiments with the Osher Upwind Scheme for the Euler Equations," AIAA Paper 82-0975, 1982.

[13] Rai, M. M., "An Implicit, Conservative, Zonal-Boundary Scheme for Euler Equation Calculations," AIAA Paper 85-0488, 1985.

[14] Dring, R. P., Joslyn, H. D., Hardin, L. W., and Wagner, J. H., "Turbine Rotor-Stator Interaction," *Journal of Engineering for Power*, Vol. 104, October, 1982.

[15] Madavan, N. K., Rai, M. M., and Gavali, S., "Grid Refinement Studies of Turbine Rotor-Stator Interaction," AIAA Paper 89-0325, 1989.

[16] Joslyn, H. D. and Dring, R. P., "Three Dimensional Flow and Temperature Profile Attenuation in an Axial Flow Turbine," UTRC Report R89-957334-1, March, 1989.